ORIGINAL ARTICLE

Response of nonconforming RC shear walls with smooth bars under quasi-static cyclic loading

Muhammed Nadir Olabi[1] ⓘ · **Naci Caglar**[2] ⓘ · **Mehmet Emin Arslan**[3] · **Hakan Ozturk**[2] · **Aydin Demir**[2] · **Gokhan Dok**[4] · **Batuhan Aykanat**[3]

Abstract

In this study, an experimental investigation is conducted to determine the behavior of RC shear walls found in old and existing buildings that do not comply with the design rules in modern earthquake standards. Scaled reinforced concrete shear wall specimens are built with smooth bars and low concrete quality. The dimensions of the shear wall specimens were selected with an aspect ratio bigger than two as 2500, 1050, and 150 mm for the height, length, and thickness, respectively. Four specimens are representative of nonconforming shear walls, and one wall is used as a reference specimen which was designed in accordance with recent building codes using deformed bars. The behavior of the shear walls is determined experimentally by displacement-lateral load relationship under lateral cyclic loading. The study used measurable parameters to investigate the behavior of the test specimens in terms of lateral force capacity, rigidity, ductility, dissipated energy, and displacement components contribution to the total lateral response of the walls. The results showed a substantial loss of stiffness, ductility and energy dissipation capabilities for the tested nonconforming shear walls. Moreover, it is proven in this study that these specimens are governed by the bar slip phenomena which demonstrated more than 80% contribution to the total lateral displacement capacity. In contrast, the reference shear wall exhibited a notable flexural behavior and plastic hinge formation. Additionally, the shear walls built with smooth reinforcement bars lost about 44% of their theoretical potential flexural capacity due to the observed bar slip failure.

Keywords Experimental study · Nonconforming RC shear wall · Smooth reinforcement bar · Cyclic load · Bar slip

1 Introduction

Considerable part of reinforced concrete (RC) buildings in many countries in highly seismic regions, like Turkey, Greece, Italy and Chile, were designed and built according to old standards, and therefore these types of structures do not meet the requirements of modern

✉ Naci Caglar
  caglar@sakarya.edu.tr

Extended author information available on the last page of the article

Fig. 1 Damaged RC columns in old buildings, smooth bar and low transverse reinforcement content (Caglar et al. 2022)

and current earthquake resistant structure design. Recent field surveys after earthquake events (Caglar et al. 2022; Di Sarno and Pugliese 2020; Palios et al. 2020; Opabola et al. 2019; Celebi et al. 2013) indicated that most of the damaged buildings were built before the application of modern earthquakes norms present low concrete quality and smooth bars (Fig. 1). Similarly, reinforced concrete walls in structures built before the Turkish regulations of 1998 (TBEC 1998) do not meet the requirements of modern seismic codes. For instance, concrete strength of these reinforced concrete walls is very low (less than 15 MPa), smooth reinforcement steel bars are generally used, and the reinforcement configuration and detailing are far from the requirements of current earthquake standards.

Many researchers have investigated shear walls with low reinforcement ratios and insufficient seismic detailing. For example, Greifenhagen and Lestuzzi (2005) and Orakcal et al. (2009) performed tests on lightly reinforced squat shear walls with aspect ratio less than one. This kind of elements are controlled by shear behavior, which is typically different from walls found in multi-story buildings that are controlled by flexure failure modes. Oh et al. (2002) studied the effect of boundary zone reinforcement detailing on the response of structural walls with aspect ratio of 2.0. Hube et al. (2014), tested slender shear walls similar to those found in damaged buildings after 2010 Maule, Chile earthquake. The experimental results of the tested walls are compatible with their anticipated theoretical flexural capacity and failed in flexure due to crushing of concrete at the compression zone. Christidis and Trezos (2017), performed an assessment study on shear walls that are not designed according to Eurocode, and concluded that the bearing capacity of the tested specimens was not affected to a big degree by the fact that the walls are nonconforming to the modern standards. Christidis and Karagiannaki (2021), investigated the displacement capacity of four cantilever medium-rise inadequately reinforced concrete shear walls, and calculated shear and flexure displacement components using the experimental results. Altheeb (2016) conducted an experimental study on RC walls which are widely used in medium and low seismic regions in Australia. The specimens in this study have one layer of the vertical and horizontal steel which is not a common practice in other highly seismic zones like Turkey and Greece. Lu et al. (2017) tested RC shear wall representing elements used in high-rise buildings in moderate earthquake zones in New Zealand. Although, the results showed that the behavior of the samples was controlled by one or two cracks at base

level which reduced the drift capacity of the shear walls, bar slip was not examined and quantified separately. Motter et al. (2018) investigated the lack of special boundary elements on the behavior of large-scale walls, and recommend modifications to the limiting parameters found in recent codes.

Noticeably, most of the researches used deformed reinforcement bars and a relatively good quality concrete (25–40 MPa) in their experimental studies, which is not the case for older buildings built with conventional methods (Caglar et al. 2022; Celebi et al. 2013). Deng et al. (2012) used low strength concrete (15 MPa) and low reinforcement ratio in their investigation, but the axial load ratio was very high ($N/(A_g F_{co}) = 35 - 55\%$) which is not common in old and existing buildings. Moreover, limited experimental data is available on the use of smooth reinforcement bars in reinforced concrete elements in general and shear walls specifically. Since the risk of bar slip is much higher in RC buildings with the existence of smooth bars and low concrete quality, it is important to examine in details the behavior of RC shear walls in such conditions to exactly determine the seismic performance of these elements.

In this study, nonconforming reinforced concrete slender shear walls built with smooth reinforcement bars and low-quality concrete are studied under quasi-static cyclic loading. An experimental program is conducted on five scaled RC shear wall specimens, one reference wall built according to modern standards (ACI318 2019; TBEC 2018), and four specimens are representative of walls found in old and existing buildings. Test results are evaluated and discussed in terms of lateral force capacity, rigidity, ductility, dissipated energy, and displacement components contribution to the total lateral deformation of the shear walls.

2 Experimental program

The experimental program was carried out in the Structural-Mechanics Laboratory at Düzce University, and consisted of five scaled reinforced concrete shear walls. One reference conforming shear wall specimen (CSW0) designed with the guidance of modern building standards (ACI318 2019; TBEC 2018), and four other specimens built with similar characteristics to reinforced concrete elements found in old existing buildings with low concrete quality, smooth bars, and lack of seismic detailing and called the nonconforming shear wall (NCSW) samples. Since the tested walls are not full-scale, the code requirements were slightly loosened for the convenience of the shear walls manufacturing.

2.1 Test specimens

Many parameters affect the behavior of RC walls under reversible lateral loads. The dimensions of the element will mostly determine the flexure or shear contribution to the total response. Cross-section properties (cover, reinforcement arrangement), the transverse and longitudinal reinforcement ratios in the boundary zone (BZ) and the web, and material properties (concrete, steel) are also very important factors that influence the strength, rigidity and energy dissipation capabilities of the studied element.

For this study, while the dimensions were kept constant for all the test specimens, reinforcement steel arrangement and ratios, and the concrete compressive strength were considered as the variable parameters to be examined. RC shear wall length to thickness ratio set to be larger than seven ($L_w/b_w \geq 7$) since it is the accepted ratio in the standards to
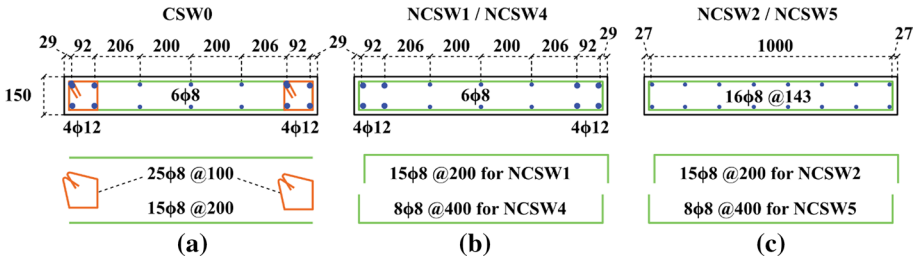
Fig. 2 Section details of the test specimens **a** deformed, **b** and **c** smooth steel bars. Dimensions in (mm)
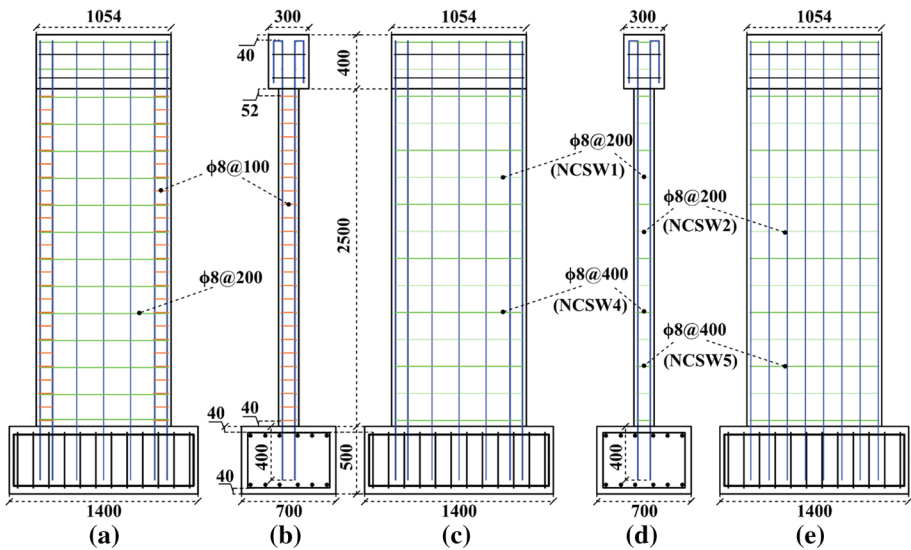

Fig. 3 Reinforcement details of the test specimens. Reference (CSW0) **a** front and **b** side sections, **c** NCSW1 and NCSW4 front sections **d** NCSW side section **e** NCSW2 and NCSW5 front section. Dimensions in (mm)

consider an RC element as shear wall. Additionally, the aspect ratio (H_w/L_w) was selected to be more than two as the focus of this study is on slender wall elements. Accordingly, the selected dimensions were $b_w = 150$mm, $L_w = 1054$mm, and $H_w = 2500$mm for the thickness, length, and height of the wall, respectively, with 15 mm clear concrete cover.

The details of the cross-section and the longitudinal and transverse steel configurations of the tested specimens are shown in Figs. 2 and 3, respectively. The reference test wall (CSW0) had a well confined columns in the boundary zone using 100 mm spaced ties, and transverse steel with 200 mm spacing. Two of the other nonconforming specimens (NCSW1 and NCSW4) used the same reinforcement steel configuration in the section as the reference wall, with concentrated boundary zone steel (CBZS) and the same bar diameters (12 mm for the boundary zone, and 8 mm in the web). The main difference was the use of smooth bars for longitudinal and transverse reinforcing steel, and the other was the absence of confinement ties. The remaining two nonconforming specimens (NCSW2 and NCSW5) used distributed longitudinal 8 mm smooth steel reinforcement bars. Two

Table 1 Matrix of the test specimens

Specimen name	Concrete quality	ρ_l^{BZ} (%)	ρ_l^{web} (%)	ρ_l^{total} (%)	ρ_h^{BZ} (%)	ρ_h^{web} (%)
CSW0 (reference)	C25	2.01	0.27	0.77	0.67	0.34
NCSW1	C14	2.01	0.27	0.77	–	0.34
NCSW2	C14	–	0.47	0.51	–	0.34
NCSW4	C14	2.01	0.27	0.77	–	0.17
NCSW5	C14	–	0.47	0.51	–	0.17

ρ_l^{BZ}: Reinforcement ratio of longitudinal steel in the boundary zone.

ρ_l^{web}: Reinforcement ratio of longitudinal steel in the web.

ρ_l^{total}: Total Reinforcement ratio.

ρ_h^{BZ}: Reinforcement ratio of transverse steel in the boundary zone.

ρ_h^{web}: Reinforcement ratio of transverse steel in the web.

Table 2 Reinforcement steel mechanical properties

Bar diameter (mm)	Bar type	f_y (MPa)	f_u (MPa)	E_s (MPa)	E_{sh} (MPa)	ε_y	ε_{sh}	ε_u	ε_f
8	Smooth	492.5	546.2	203,050.0	1827.5	0.0031	–	0.0634	0.1055
12	Smooth	381.2	461.8	231,258.0	3468.8	0.0022	0.0199	0.1233	0.1706
8	Deformed	436.8	585.7	200,770.0	3929.3	0.0029	0.0147	0.1518	0.2302
12	Deformed	457.1	580.6	244,568.0	4891.4	0.0022	0.0255	0.1115	0.1153

different transverse steel spacings were used in the NCSW samples (400 and 200 mm) to reproduce different built conditions in old and existing buildings. Concrete quality was also one of the main differences between the reference shear wall and the NCSW specimens. Low quality concrete mix with 14 MPa compressive strength at 28 days (C14) was prepared to be used for the nonconforming shear walls to re-create old RC elements properties, and normal quality concrete (C25) was used for the reference specimens. Table 1 shows the matrix of the shear walls specimens with reinforcement ratios calculated according to ACI318 (2019) section R18.10.6.5.

2.2 Material properties

Two types of reinforcement were used to build the test shear wall specimens, smooth and deformed steel bars. Also, for each type two diameter sizes, 8 and 12 mm, were used. Three 400 mm long samples of each kind of the reinforcement steel were tested to determine their average mechanical properties and presented in Table 2. The test performed according to ASTM E8/E8M-15a (2015) using a 50 mm strain gauge extensometer. Table 2 shows the yield (f_y) and maximum stress (f_u) and the corresponding strains ε_y and ε_u values, respectively. Also, the modulus of elasticity (E_s), hardening strain (ε_{sh}), and tangent modulus at onset of strain hardening (E_{sh}) are given in the table. The ultimate strain, ε_f, of the tested samples are calculated at the point where the stress value drops to 90 percent of the maximum stress (f_u). Stress–strain relationships for the four types of the tested steel bars are given in Fig. 4.

Fig. 4 Stress–strain relationships for steel bars used in the experiment, **a** 8 mm smooth, **b** 12 mm smooth, **c** 8 mm deformed and **d** 12 mm deformed reinforcement bars
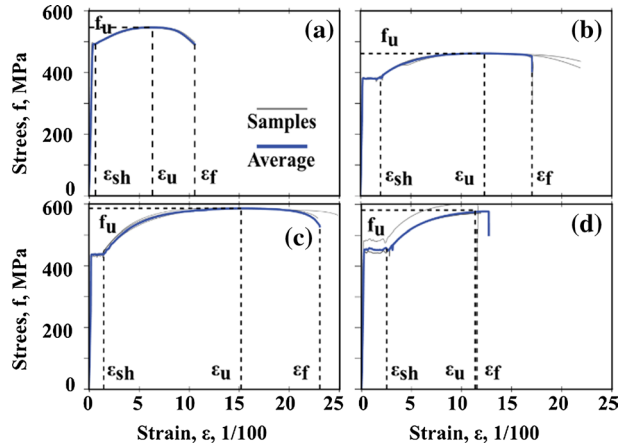
Concrete specimens were taken and prepared during the pouring of the tested shear walls. Minimum of three cylinder and three cubic specimens were tested and the obtained average results shown in Table 3. Cylinder strength (f_c') was determined from a 150×300 mm molds, and the cubic strength (f_c^{cube}) determined from cube molds with a 150 mm edge length. Concrete modulus of elasticity (E_c) was obtained using the cylinder specimens and the resulted stress–strain relationships are presented in Fig. 5. The compressive test was performed in the same day as the corresponding shear wall sample was tested, and the age of the concrete in the test day is also shown in Table 3.

Table 3 Concrete mechanical properties

Specimen name	Concrete age (days)	f_c^{cube} (MPa)	f_c' (MPa)	E_c (GPa)
CSW0	106	45.7	27.5	25.5
NCSW1	199	21.4	15.2	18.7
NCSW2	119	14.8	11.8	16.5
NCSW4	241	21.4	15.2	18.7
NCSW5	271	20.2	14.7	18.6

Fig. 5 Stress–strain relationships for the concrete used in the experiment
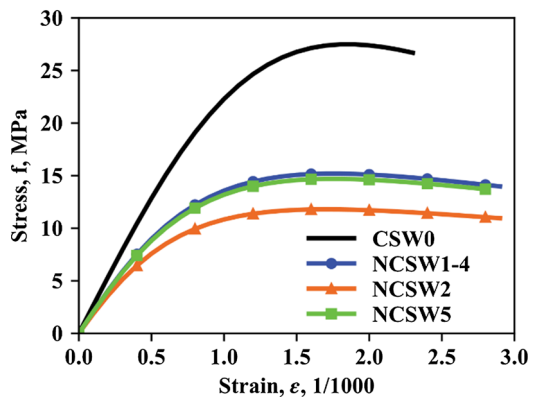
2.3 Test setup and instrumentation

The concrete of every tested shear wall was poured in one stage, including the base and the loading beam, while the specimen was laid horizontally to ensure a correct placement of the concrete. And after curing for at least 28 days the shear walls were placed into upright position till the day of the experiment. In the test setup used in this study, only lateral load was applied and the axial force was assumed to be equal to zero. Generally, the normalized axial load values in shear walls are small $(N/(A_g f_{co}) \leq 0.1)$ especially in old buildings with few stories. Therefore, axial loads with ratios less than 10 percent have a minimal effect on the behavior of flexure-controlled shear walls (Christidis and Trezos 2017; Shegay et al. 2018). Accordingly, axial loads were not considered within the scope of the current experimental study to eliminate any effect on the observation of bar slip behavior expected in the test specimens. At the beginning of the test, the specimens were mounted to the rigid floor as seen in Fig. 6, and a cyclic lateral load was applied using a 500 kN capacity servo-controlled actuator connected to the reaction wall.

The responses of the tested shear walls under quasi-static cyclic loads were monitored using an array of linear potentiometer on the surface, and strain gauges fixed on the steel bars before casting the walls. A total of 18 linear potentiometer displacement transducers (LPDT) were used in the experimental setup to measure the global and local deformations. Three of them were used to measure the global lateral displacement of the tested specimen on three different levels, as seen in Fig. 6a. Four LPDTs placed in diagonal X shaped configuration over two levels were used to measure the shear displacements in the tested walls. Moreover, the flexure displacement was measured with the help of six potentiometers placed vertically along the height of the wall to measure the relative vertical deformation between the levels. Two more devices were placed on both sides of the wall and fixed at 300 mm height from the surface of the base, to measure the rotation of the wall at base level, mostly due to reinforcement bar slippage. Three other spring-return linear potentiometers were used to control the potential horizontal sliding and rotation of the concrete foundation of the wall.

Local deformations of the reinforcement steel were measured using twelve strain gauges distributed in critical points. Four gauges were located at near base level (inside the plastic zone), four inside the concrete foundation to measure the possible strain penetration. Two other strain gauges were placed outside the possible plastic zone at 600 mm height from the surface of the base. The last two devices were used to measure the strains for the transverse reinforcement bars (one inside and one outside the potential plastic zone).

In addition, one 500 kN capacity load cell was used to measure the applied lateral load from the actuator. Load and displacement values collected during the experiments were transferred to a computer system with the help of a 32-channel static data logger with 0.125 Hz sampling rate.

In order to prevent any out-of-plane displacements that could affect the test results, a newly fabricated steel braced frame system was installed on both sides of the tested wall. Furthermore, the upper loading beam was supported through roller wheels contacting the surface of the beam to ensure the continuity of the lateral movement at the support point. Figure 6d shows the out-of-plane support system and the rolling support wheels.

A displacement-controlled loading protocol was used in this experimental study based on the recommendation from ACI 374.2R (2013). Two cycles at each drift level were applied as shown in Fig. 7 with 0.075, 0.15, 0.25, 0.5, 1.0, 1.5, 2.0, 2.5, 3.0, and 4.0% drift ratios.
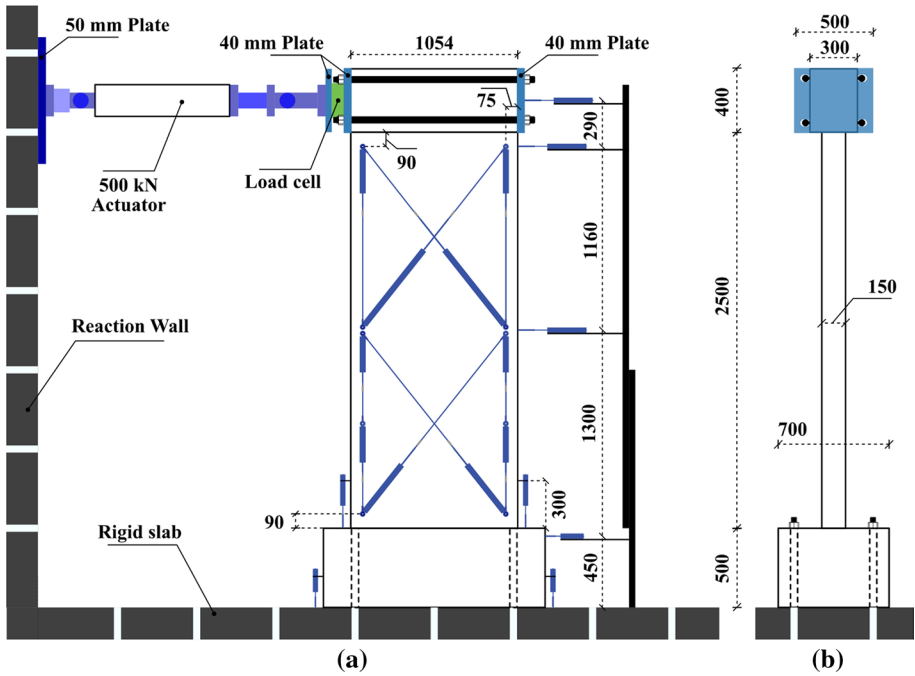
Fig. 6 Instrumentation setup used in the experiment, **a** front and **b** side views, **c** Linear potentiometer locations, **d** Out-of-plane support system and rolling wheels. Dimensions in (mm)

3 Test observations

3.1 Reference specimen, CSW0

The cyclic lateral load–displacement curve of the CSW0 specimen (reference) is given in

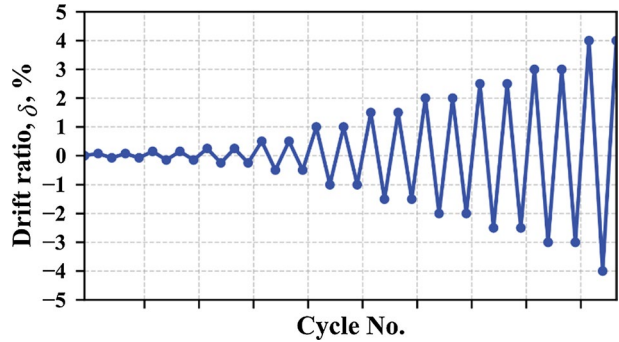**Fig. 7** Cyclic quasi-static load protocol

Fig. 8. In addition, crack patterns of the reference specimen at the end of the experiment are shown in Fig. 9. As seen in Fig. 8, the maximum load and the corresponding displacement values were measured as + 105.93 kN and 37.00 mm (+ 1.37% drift ratio) when pulled in the positive direction, and + 109.29 kN and + 19.90 mm (+ 0.74% drift ratio) when pushed in negative direction, respectively. The first tensile crack was observed at a load of + 39.44 kN and a corresponding displacement of + 2.30 mm (+ 0.09%). First reinforcement yield was detected at a load of − 103.90 kN and a corresponding displacement value of − 16.30 mm (− 0.60% drift ratio), this yield ($\varepsilon_y = 0.0022$) was observed in the bar with a strain gauge labeled B1i (Fig. 13b). In succeeding stages and while the load increases, cracks started to form at different levels and the width and length of the previously formed cracks started to increase. The first crack formed at the base surface occurred at a displacement level of − 29.40 mm (− 1.09%) and a corresponding load value of − 103.10 kN. When the applied displacement reached + 48.05 mm (+ 1.78% drift ratio), the concrete cover started to break and spalling was observed. Consequently, within the same cycle in the opposite direction, bar buckling was first observed at − 64.50 mm (− 2.39%) displacement level. As seen from Fig. 8, the negative side showed a faster degradation compared to the positive side. This was the result of local damage (cracks, concrete spalling and bar buckling) was firstly observed and developed significantly afterwards at this side of the wall (Fig. 9). Moreover, due to the increase of confinement force with higher drift ratios, the

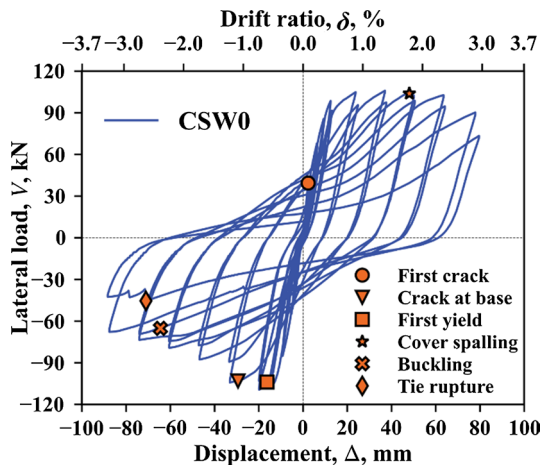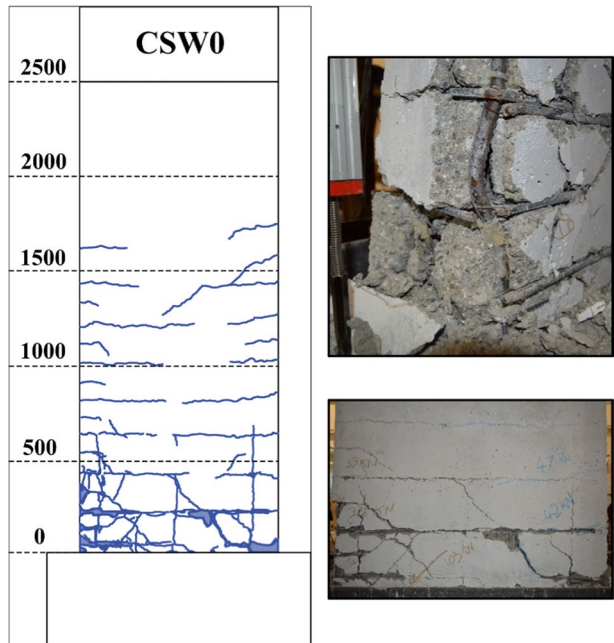**Fig. 8** Cyclic quasi-static response of the reference specimen

Fig. 9 Crack patterns of the reference specimen at the end of the experiment. Dimensions in (mm)

first stirrup rupture occurred at −71.05 mm (−2.63%) displacement. A couple more stirrups in the boundary zones broke afterwards sequentially, and the experiment was stopped at this point to prevent dangerous instabilities in the element. At the end of the experiment, plastic hinge length was measured according to concrete cover spalling and damaged region starting from the base surface and estimated as 34.0 cm.

The specimen CSW0 showed a dominant flexural behavior, which can be seen clearly from the cracks pattern directions and propagation. A substantial amount of the cracks were horizontal with very few of them spread diagonally, which indicates that the contribution of shear component to the total displacement was slightly small. Moreover, since a large crack formed relatively early at the base surface (1% drift ratio), the bar slip contribution to the total displacement is considered to be quite essential. The displacement components of all the tested specimens will be discussed comprehensively later in this paper.

3.2 Nonconforming specimens, NCSW

The cyclic lateral load–displacement relationships of the nonconforming shear wall specimens are given in Fig. 10. In the figure the points where the first crack and the crack at the base level first started are marked. For **NCSW1** the first observable crack was detected at +2.59 mm (+0.10%) deformation and +10.58 kN load value. The maximum load was achieved with +39.83 kN in the pull direction and -50.25 kN in the push direction with corresponding displacement values of +14.20 mm (+0.53% drift ratio) and −14.82 mm (−0.55%), respectively. When the maximum load value was reached, one big crack started to form at the surface of the foundation. In **NCSW2** test specimen, the first crack was observed at +2.49 mm (+0.09%) displacement with 11.04 kN lateral load value. The maximum load was reached at −5.76 mm (−0.21%) in the push direction and +8.77 mm
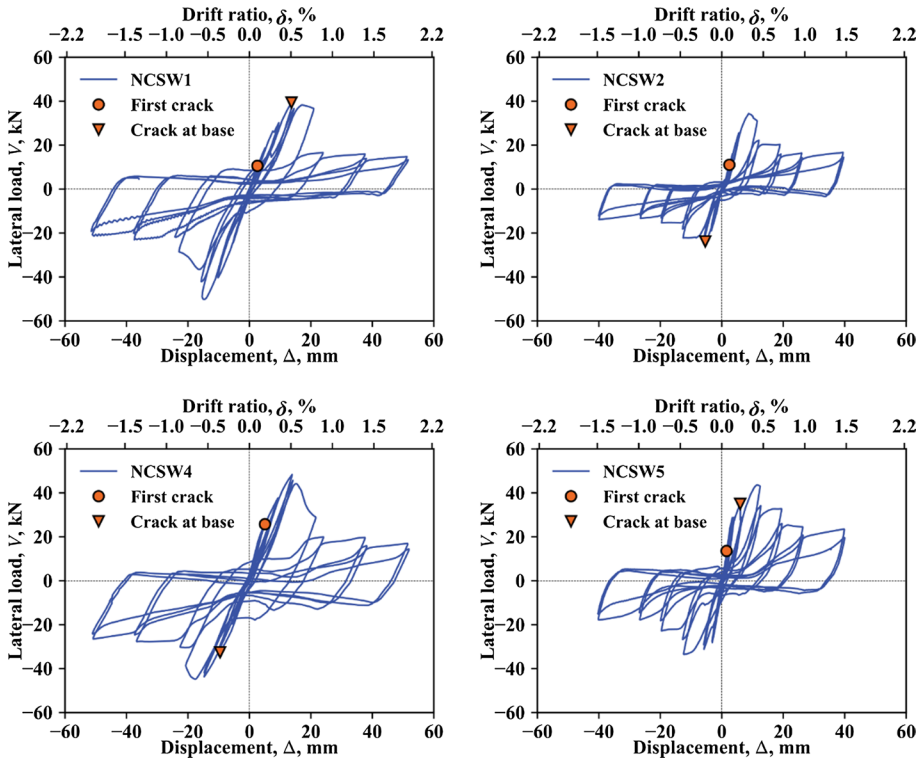
Fig. 10 Cyclic quasi-static response of the tested nonconforming shear walls

(+0.32%) in the pull direction with corresponding force values of −24.87 kN and +34.37 kN, respectively. The crack at the base level begun its formation at the same drift levels of the maximum lateral load value. Similarly, for **NCSW4** the first crack was observed at +5.04 mm (+0.19%) displacement with 25.75 kN lateral load value. At −0.35% drift ratio (-9.55 mm displacement) a crack was observed at the surface of the base with −32.57 kN lateral force level. The maximum load reached −44.78 kN and +48.33 kN for the push and pull directions, respectively. The displacement at the maximum load were −17.61 mm (−0.65% drift ratio) and +13.89 mm (+0.51%) for the push and pull directions, respectively. Likewise, the first and only crack in the body of **NCSW5** test specimen was observed at +13.57 kN lateral load value with +1.54 mm (+0.06%) deformation. The crack at the base level started to form at +35.02 kN load level and +5.99 mm (+0.22% drift ratio) displacement. The maximum load was achieved with +43.61 kN in the positive pull direction and −33.53 kN in the negative push direction with corresponding displacement values of +11.46 mm (0.42% drift ratio) and −12.31 mm (−0.46%), respectively.

Table 4 summarizes the main failure events occurred during the test for the walls with their drift ratios. Moreover, crack patterns of all the NCSW specimens at the end of the experiment are shown in Fig. 11. Also, Fig. 12 shows an example of the big crack that formed at the base level in all the nonconforming shear walls. As seen from the figures, very few cracks have occurred during the experiment (3 to 4 for the shear walls with CBZS, and only one for the specimens with distributed reinforcement). All the

Table 4 Drift ratios at main failure events (%)

Specimen	First crack	Yield	Crack at base	Cover spalling	Buckling	Tie rupture
CSW0	+0.09 @39.44 kN	−0.60	−1.09	+1.78	−2.39	−2.63
NCSW1	+0.10 @10.58 kN	–	+0.53	–	–	–
NCSW2	+0.09 @11.04 kN	–	−0.21	–	–	–
NCSW4	+0.19 @25.75 kN	–	−0.35	–	–	–
NCSW5	+0.06 @13.57 kN	–	+0.22	–	–	–
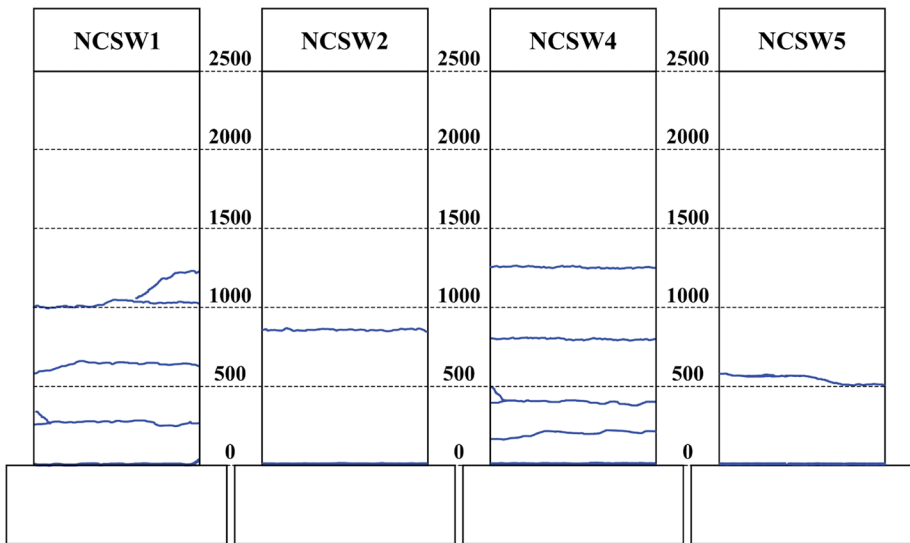
Fig. 11 Crack patterns of the nonconforming shear walls at the end of the experiment. Dimensions in (mm)

cracks started before the observation of the big crack at the base surface, and none have been seen after that point. Additionally, the response of the NCSW specimens showed a big drop in lateral capacity after the creation and propagation of the crack at base level, and the behavior in the following cycles was controlled by rigid body rotation. It was obvious that the reinforcement bar-concrete adherence was lost due to the use of smooth steel and significant bar slip was observed. Furthermore, few of the longitudinal reinforcement (most-outer bars) reached their yield point, and none of the bars inside the base yielded, which indicated the fundamental loss of adherence. Figure 13c and d presents the variations of the strain in the reinforcement during the experiment for the nonconforming specimens NCSW1 and NCSW2. Since the behavior was dominated by bar slip, concrete crushing or cover spalling was not observed in the compression zone, and the lateral shear reinforcement variations exhibited a negligible contribution to the total response of the shear walls built with smooth bars. Moreover, after the significant drop in strength of the NCSW specimens, two more drift levels were applied till the lateral capacity was settled at a residual lateral force about 22.0, 16.7, 20.1, and 23.8 kN for the specimens NCSW1, NCSW2, NCSW4, and NCSW5, respectively, and the experiment was ended there.
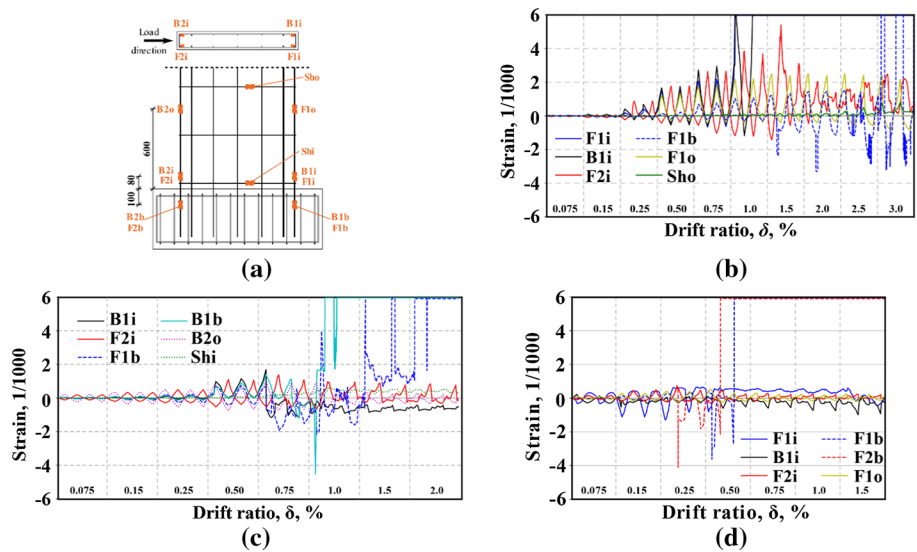
Fig. 12 Crack at base level in specimen NCSW2

Fig. 13 **a** Strain gauge locations and configurations, and change of strain values during the test for **b** CSW0 **c** NCSW1 and **d** NCSW2

4 Discussion of the test results

4.1 Test results evaluation

For the purpose of providing quantitative evaluation of the total behavior of the tested shear walls under cyclic loads, the lateral force strength, stiffness of the element, ductility, and the amount of dissipated energy are calculated.

According to the definitions from Fig. 14a, V_{max} and Δ_{max} are the maximum lateral force capacity of the shear wall specimen and the corresponding displacement, respectively. The ultimate drift capacity, Δ_u, is adopted to be the displacement reached before
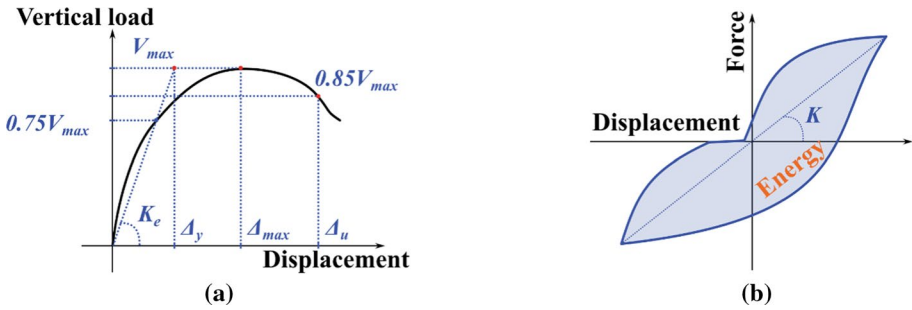
Fig. 14 **a** Definition of effective stiffness and main drifts figures on the lateral load–displacement envelope, **b** dissipated energy and stiffness calculation for one loop

losing 15% of the maximum strength (Murty et al. 2012; Zhang et al. 2014). The effective stiffness of the element, K_e, is calculated according to ACI 374.2R (2013), where it is acknowledged as the slope of the line between the origin and 75% of the maximum strength (Fig. 14a). Moreover, the yield displacement, Δ_y, is determined as the projection of the intersection point of the line starting from origin with K_e slope and the horizontal line at V_{max} level. Additionally, the cumulative dissipated energy, E_h, of the specimens is calculated as the sum of the areas defined by each of the loop curves of the lateral load–displacement relationship as seen from Fig. 14b.

To take into account both of the positive and negative direction in the evaluation study, the ductility, μ, and the element stiffness, K, are calculated as per Eqs. (1) and (2), respectively (Razvi and Saatcioglu 1994). This method is also used to determine the stiffness degradation of the wall specimen under quasi-static cyclic loads. The average secant stiffness of each loop is calculated using Eq. (2) and by considering the positive and negative peak points of the loop, as seen in Fig. 14b.

$$\mu = \frac{\left|\Delta_u^+\right| + \left|\Delta_u^-\right|}{\left|\Delta_y^+\right| + \left|\Delta_y^-\right|} \tag{1}$$

$$K = \frac{\left|V_{max}^+\right| + \left|V_{max}^-\right|}{\left|\Delta_y^+\right| + \left|\Delta_y^-\right|} \tag{2}$$

The resulted data are summarized and tabulated in Table 5 showing the main backbone figures in both directions (negative and positive) for each specimen with the average ductility, average rigidity, and cumulative dissipated energy (E_h). As seen from the table, all the tested shear walls with smooth reinforcements bars fall significantly behind the reference specimen with deformed bars in all performance terms, with an average of 2.6 and 2.0 times for the ductility and rigidity, respectively, and 12.3 times less in the total amount of dissipated energy.

Envelops of the lateral load–displacement relationship for all the specimens are presented in Fig. 15a. Comparing the curves of the nonconforming shear walls (NCSW) with the reference shows that the adhesion between the smooth reinforcement bars and the concrete was lost rapidly and the bars started to slip from the concrete base before

Table 5 Experimental results

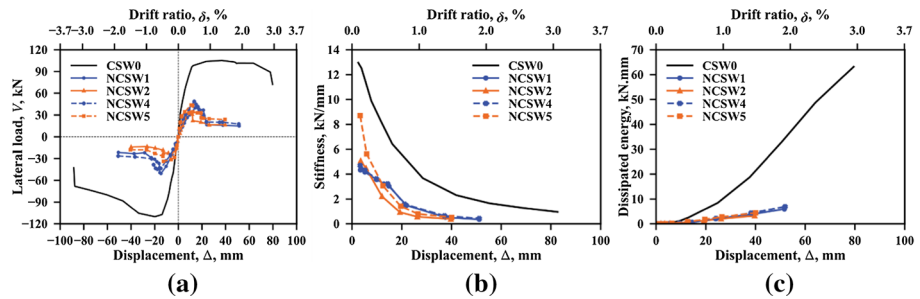| Specimen name	Δ_y (mm)	Δ_{max} (mm)	V_{max} (kN)	Δ_u (mm)	μ	K (kN/mm)	E_h (kN.m)
CSW0	+ 10.92	+ 37.00	+ 105.93	+ 77.86	5.29	9.51	63.20
	− 11.70	− 19.90	− 109.29	− 41.85			
NCSW1	+ 12.60	+ 14.20	+ 39.83	+ 21.61	1.51	3.63	5.93
	− 12.23	− 14.82	− 50.25	− 15.83			
NCSW2	+ 7.95	+ 8.77	+ 34.37	+ 11.92	1.98	4.77	3.22
	− 4.47	− 5.76	− 24.87	− 12.68			
NCSW4	+ 11.65	+ 13.89	+ 48.33	+ 16.86	1.48	3.63	6.92
	− 14.03	− 17.61	− 44.78	− 21.04			
NCSW5	+ 7.08	+ 11.46	+ 43.61	+ 12.31	2.38	7.27	4.40
	− 3.53	− 12.31	− 33.53	− 12.90			

Fig. 15 Comparison of **a** response envelope, **b** stiffness degradation, and **c** energy dissipation

yielding. This behavior has significantly reduced the load carrying capacity of the non-conforming shear walls compared to the reference specimen.

Stiffness degradation is compared for all the test walls in Fig. 15b. The greatest effective stiffness was obtained for the reference specimen (CSW0) due to the high strength of concrete and the contribution of the deformed bars. In addition, the test specimens built with distributed reinforcement (NCSW2 and NCSW5) showed a relatively high initial stiffness, since only one crack was formed and behaved similar to non-cracked sections. After the formation of the big crack at base surface the stiffness decreased rapidly compared to the walls with concerted boundary zone steel.

The energy dissipation capacities of NCSW specimens, that experienced slippage of the longitudinal reinforcements before reaching the yield limit, are substantially at lower levels than the reference shear wall (CSW0). The cumulative energy dissipation of the tested specimens is given in Fig. 15c. The figure shows that the dissipated energy of the reference shear wall reaches 60 times the energy dissipated by the nonconforming specimens when compared at the ultimate displacement level. Additionally, when the NCSW specimens are compared against each other, it is seen again that the energy dissipation is higher in the shear walls with concentrated boundary zone steel.

It is important to notice that the bar slip is dependent on the anchorage length within the foundation, and the results may also change in relation to it. Nevertheless, the results in this paper are consistent since a relative comparison was made between shear walls built with

deformed and smooth bars with the same anchorage length. It is very important to study the response of RC shear walls by taking the anchorage type and length of the smooth bars into consideration in future studies.

4.2 Displacement components

The tested nonconforming shear walls showed a significant contribution of bar slip to the total lateral load displacement. To properly investigate this phenomenon, the total displacement should be broken down into its main ingredients. Three-component approach was adapted in this study, where the total deformation of the wall can be described as the sum of three different parts, flexure, shear, and bar slip displacements (Fig. 16a).

Based on the instrumentation configuration used in the experimental study, the tested specimens is divided into two levels identified by the X shaped LPDTs. This kind of setup is used commonly to measure the shear displacement component of the lateral deformation. However, a modification should be applied to the founded values to determine the correct shear displacement (Massone and Wallace 2004). In this work, the shear and flexure deformations are estimated according the corrections proposed by Massone and Wallace (2004). As seen from Fig. 16b, the displacement occurred at each level due to shear (U_s) and flexure (U_f) deformations is calculated using Eq. (3).

$$U_s + U_f = \frac{\sqrt{X_2^{meas2} - (h + v_1)^2} - \sqrt{X_1^{meas2} - (h + v_2)^2}}{2} \tag{3}$$

In this equation, v_1 and v_2 are the measured local deformations (change in the length of the corresponding LPDT) at the top of the level for both sides, X_1^{meas} and X_2^{meas} are the diagonal lengths of the LPDTs in the X configuration measured during the test, and h is the height of the level. Moreover, Eq. (4) is used to determine the flexural deformation
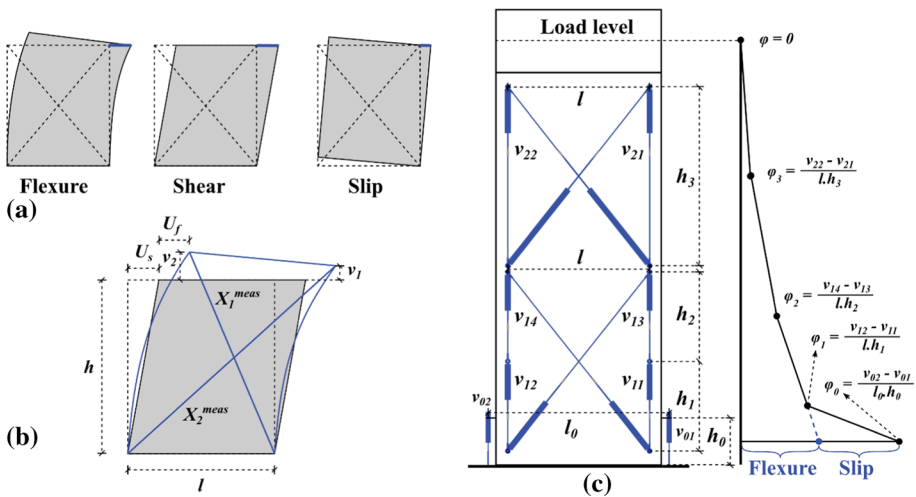

Fig. 16 **a** Three displacement components model and deformation calculations for **b** shear, flexure, and **c** bar slip displacements

for the level, where θ is the rotation in that level and calculated using Eq. (5). The length between the vertical LPDTs is l, and α is taken 0.67 as the curvature distribution is assumed to be triangular along the studied level.

$$U_f = \alpha . \theta . h \tag{4}$$

$$\theta = \frac{v_2 - v_1}{l} \tag{5}$$

The contribution of the bar slippage to the total lateral displacement of the tested specimen was obtained using the methodology described by Sezen and Moehle (2006). Figure 16c shows the estimated curvature distribution along the element, where the average curvature at each level is determined as:

$$\varphi_i = \frac{v_{i2} - v_{i1}}{l_i h_i} \tag{6}$$

The calculated curvature at the bottom of the shear wall is assumably produced from the interference of both flexural and strain penetration effects. For that reason, and to isolate the two parts, the obtained curvature in higher levels is extended linearly towards the base level approximating the flexural component, and the remaining value was expected to be as a result from slip rotation (Fig. 16c). The slip component of the total displacement is calculated by multiplying the generated slip rotation by the total height of the wall. The resulted ratios of the three displacement components are summarized in Fig. 17. In the figure, each part was divided by the sum of the three components showing the percentage of the contribution of this part from the total deformation.

From the figure, it is clear that the governing displacement component for the nonconforming shear walls is the part which formed from the bar slip phenomena. This component is usually noticeable, for all the NCSW specimens, after creating the big crack at the base surface, and a significant drop of strength is observed after reaching the maximum lateral force (Fig. 10). For instance, the flexural part of the displacement for NCSW1 is about 79% when V_{max} is reached and crack-at-base is formed, and drops to 16% at the next drift level, while the slip component increases from 8 to 80% for the same drift ratios. In a same manner, slip-displacement rises 36, 51, and 56% after crack-at-base formation for the specimens NCSW2, NCSW4, and NCSW5, respectively. And after this stage, the slip-displacement component contributes about 97% to the total deformation. In addition, the test specimens with CBZS showed a slightly more flexural behavior than the walls with distributed reinforcement. All the nonconforming shear walls exhibited a minimal shear behavior, and the shear-displacement contribution was very small compared to the other two parts.

On the other hand, the reference shear wall sustained a notable flexural behavior throughout all the experiment stages and formed a pronounced plastic hinge, with non-negligible shear and slip contribution to the total lateral deformation. The flexural displacement at V_{max} is 68.3%, while the shear and slip parts are 13.7 and 18.1%, respectively. Although, the CSW0 exhibited a crack formation at the base level, the flexural displacement contribution to the total deformation is dropped only 15.2%, and the slip part increased 11.3%. The displacement components contributions at the end of the test are 37.6, 31.1, and 31.4% for the flexure, shear, and slip displacements, respectively.
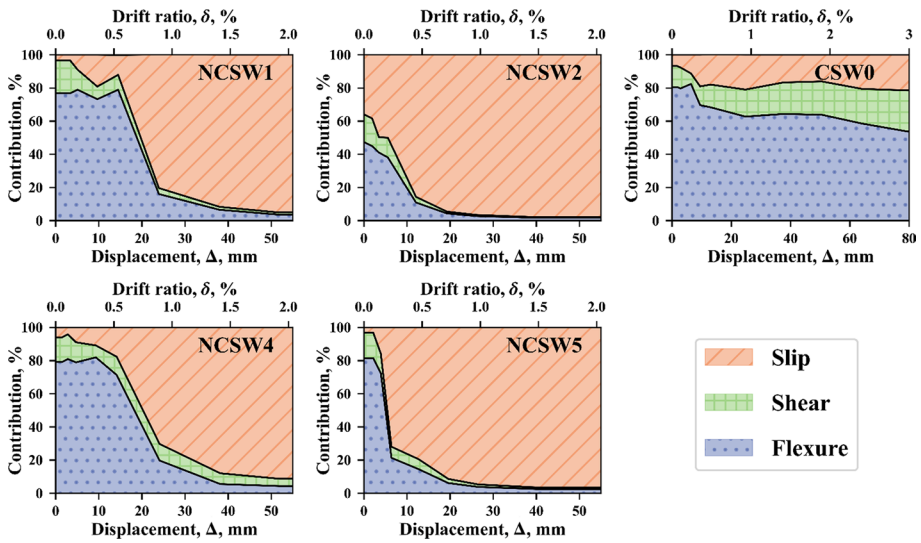
Fig. 17 Displacement components contribution to the total lateral displacement

4.3 Theoretical analysis

The experimental strength values acquired during the test are compared to theoretical results obtained from modern earthquake standards (ACI318 2019; TBEC 2018) and from moment–curvature analysis. The shear strength (V_r) for shear walls was calculated according to Sect. 7.6.7 from the Turkish standard (TBEC 2018), which is similar to the shear strength defined in Sect. 11.5.4.3 of ACI 318 (2019). For the moment–curvature analysis, a previously developed numerical code (Caglar et al. 2019) was adopted and modified for shear walls. The code uses a fiber based sectional analysis to calculate the maximum moment capacity for each test specimen. And since the tested shear walls are working as cantilever elements, the lateral force capacity (V_f) is determined by dividing the obtained maximum moment by the height of the lateral load (2700 mm). While V_r is bigger than V_f in all cases, Table 6 shows the results of the comparison study with ratios of the maximum shear force found experimentally (V_{exp}) to the potential strengths found from the curvature-moment analysis and standard equations. From the table, it can be seen clearly that the nonconforming shear walls exhibit significant loss in their shear force due to bar slip, with an average reduction ratio of 44%.

5 Summary and conclusions

This work presents the experimental results of five scaled shear walls tested under lateral cyclic quasi-static loading. Four specimens built with smooth bars and low concrete quality to represent the walls found in old and existing buildings, and one shear wall designed and built according to modern earthquake codes.

The behavior of the shear wall specimens in this study were examined in terms of lateral force capacity, rigidity, ductility, dissipated energy, and displacement components contribution to the total lateral deformation of the walls. Also, the response of the nonconforming

Table 6 Experimental and theoretical results comparison

Specimen name	V_{exp} (kN)	V_f (kN)	V_r (kN)	$\dfrac{V_{exp}}{V_f}$	$\dfrac{V_{exp}}{V_r}$
NCSW1	50.25	88.39	389.05	0.57	0.13
NCSW2	34.37	67.53	373.81	0.51	0.09
NCSW4	48.33	88.39	259.02	0.55	0.19
NCSW5	43.61	69.50	256.89	0.63	0.17
			Average	0.56	0.15
CSW0	109.29	107.04	403.87	0.98	0.27

shear walls was compared with the response of the reference specimens based on quantitative characteristics obtained from the test results. The conclusions of the experimental study are summarized as follows:

- When examining all the tested shear wall specimens, it is concluded, that the concrete strength and the surface properties of the used reinforcement are significantly affecting the behavior of the walls. The experimental study showed that while flexural response was dominant in the reference specimen CSW0, that was built with deformed steel bars, the NCSW specimens built with smooth reinforcement showed a very clear bar slip controlled response.
- Although few more cracks observed at transverse reinforcement levels in the shear walls with concentrated steel reinforcement at the boundary zone, the greatest damage occurred at the wall-foundation joint surface for all the NCSW specimens. For that matter, the transverse reinforcement ratio did not have any noticeable contribution to the response of the nonconforming walls. On the other hand, flexure cracks were more common and have been formed clearly in the reference specimen (CSW0) built with deformed steel bars. Furthermore, in contrast with the NCSW specimens, longitudinal reinforcement bars showed a plastic behavior after yielding, and in advanced loading cycles buckling was observed after concrete cover spalling.
- The lateral load capacity and ductility of the nonconforming shear walls have significantly decreased due to bar slip affect in comparison with the seismically conforming specimen that showed an expected behavior similar to the theoretical values from recent design standards. For instance, the strength of the NCSW samples is reduced between 54 and 69%, and the displacement ductility is also decreased between 55 and 72% compared to the reference shear wall. Additionally, the nonconforming specimens exhibited only 56% of their potential theoretical flexural capacity due to the observed bar slip failure.
- Similarly, the reinforcement bar slippage negatively affected the rigidity and the energy dissipation capabilities of the specimens built with smooth bars and low-quality concrete. The reduction was about 50% and 92% on average for the effective stiffness and dissipated energy, respectively. Also, the shear walls with concentrated steel in the boundary zone showed higher energy dissipation values, and slower degradation in stiffness than the walls with distributed reinforcement.
- Examining the displacement components contribution to the total lateral deformation of the test shear walls confirmed that the response of the NCSW samples is controlled by reinforcement bar slip, which contributes more than 80% of the total lateral displacement capacity after reaching the maximum horizontal load. In contrast, the reference specimen CSW0 exhibited a notable flexural behavior and plastic hinge formation, with

68.3, 13.7, and 18.1% displacement contribution for the flexure, shear, and slip components, respectively, at the maximum lateral load level.

This study indicates that reinforcement bar slip is the dominant effect that dictates the overall behavior of nonconforming shear walls built with smooth bars and low-quality concrete. For this reason, these properties should be considered carefully while examining existing structures and test results could be used as a guideline in designing solutions for old buildings.

Declarations

References

ACI 374.2R (2013) Guide for testing reinforced concrete structural elements under slowly applied simulated seismic loads. In: 374.2 R-13. American concrete institute

ACI318 (2019) Building code requirements for structural concrete (ACI 318–19) and commentary (ACI 318r-19). In: American concrete institute

Altheeb AH (2016) Seismic drift capacity of lightly reinforced concrete shear walls [PhD Dissertation]. The University of Melbourne

ASTM E8/E8M-15a (2015) Standard test methods for tension testing of metallic materials. ASTM International

Caglar N, Sezen H, Olabi MN (2019) Numerical evaluation of core concrete quality on the response of concrete jacketed columns. Rev Constr 18(2):301–310. https://doi.org/10.7764/RDLC.18.2.301

Caglar N, Kirtel O, Vural I, Saribiyik A, Sumer Y (2022) Structural damages observed in buildings during the January 24, 2020 Elazig-Sivrice earthquake in Turkey. GRAĐEVINAR J Croat Assoc Civ Eng

Celebi E, Aktas M, Caglar N, Özocak A, Kutanis M, Mert N, Özcan Z (2013) October 23, 2011 Turkey/Van–ercis earthquake: structural damages in the residential buildings. Nat Hazards 65(3):2287–2310. https://doi.org/10.1007/s11069-012-0478-9

Christidis KI, Karagiannaki D (2021) Evaluation of flexural and shear deformations in medium rise RC shear walls. J Build Eng 42:102470

Christidis KI, Trezos KG (2017) Experimental investigation of existing non-conforming RC shear walls. Eng Struct 140:26–38. https://doi.org/10.1016/j.engstruct.2017.02.063

Deng KL, Pan P, Shi YY, Miao QS, Li WF, Wang T (2012) Quasi-static test of reinforced concrete shear wall with low concrete strength and reinforcement ratio. Appl Mech Mater 188:106–111. https://doi.org/10.4028/www.scientific.net/AMM.188.106

Di Sarno L, Pugliese F (2020) Numerical evaluation of the seismic performance of existing reinforced concrete buildings with corroded smooth rebars. Bull Earthq Eng 18(9):4227–4273. https://doi.org/10.1007/s10518-020-00854-8

Greifenhagen C, Lestuzzi P (2005) Static cyclic tests on lightly reinforced concrete shear walls. Eng Struct 27:1703–1712. https://doi.org/10.1016/j.engstruct.2005.06.008

Hube MA, Marihuén A, de la Llera JC, Stojadinovic B (2014) Seismic behavior of slender reinforced concrete walls. Eng Struct 80:377–388. https://doi.org/10.1016/j.engstruct.2014.09.014

Lu Y, Henry RS, Gultom R, Ma QT (2017) Cyclic testing of reinforced concrete walls with distributed minimum vertical reinforcement. J Struct Eng 143(5):04016225. https://doi.org/10.1061/(ASCE)ST.1943-541X.0001723

Massone LM, Wallace JW (2004) Load-deformation responses of slender reinforced concrete walls. ACI Struct J 101(1):103–113

Motter CJ, Abdullah SA, Wallace JW (2018) Reinforced concrete structural walls without special boundary elements. ACI Struct J 115(3):723–733. https://doi.org/10.14359/51702043

Murty CVR, Goswami R, Vijayanarayanan AR, Mehta VV (2012) Some concepts in earthquake behaviour of buildings. Gujarat State Disaster Management Authority, Government of Gujarat

Oh Y-H, Han SW, Lee L-H (2002) Effect of boundary element details on the seismic deformation capacity of structural walls. Earthq Eng Struct Dyn 31(8):1583–1602. https://doi.org/10.1002/eqe.177

Opabola EA, Elwood KJ, Oliver S (2019) Deformation capacity of reinforced concrete columns with smooth reinforcement. Bull Earthq Eng 17(5):2509–2532. https://doi.org/10.1007/s10518-018-00540-w

Orakcal K, Massone LM, Wallace JW (2009) Shear strength of lightly reinforced wall piers and spandrels. ACI Struct J 106(4):455–466

Palios X, Strepelias E, Stathas N, Fardis MN, Bousias S, Chrysostomou CZ, Kyriakides N (2020) Experimental study of a three-storey concrete frame structure with smooth bars under cyclic lateral loading. Bull Earthq Eng 18(13):5859–5884. https://doi.org/10.1007/s10518-020-00900-5

Razvi SR, Saatcioglu M (1994) Strength and deformability of confined high-strength concrete columns. Struct J 91(6):678–687. https://doi.org/10.14359/1499

Sezen H, Moehle JP (2006) Seismic tests of concrete columns with light transverse reinforcement. ACI Struct J 103(6):842–849. https://doi.org/10.14359/18236

Shegay AV, Motter CJ, Elwood KJ, Henry RS, Lehman DE, Lowes LN (2018) Impact of axial load on the seismic response of rectangular walls. J Struct Eng 144(8):04018124. https://doi.org/10.1061/(ASCE)ST.1943-541X.0002122

TBEC (1998) Specification for structures to be built in disaster areas. Ministry of Public Works and Settlement

TBEC (2018) Turkey Earthquake building regulations. Disaster and Emergency Management Presidency (AFAD), Ministry of Public Works and Settlement

Zhang H, Dong J, Duan Y, Lu X, Peng J (2014) Seismic and power generation performance of u-shaped steel connected PV-shear wall under lateral cyclic loading. Int J Photoenergy 2014:1–15. https://doi.org/10.1155/2014/362638

Authors and Affiliations

Muhammed Nadir Olabi[1] [ORCID] · **Naci Caglar[2]** [ORCID] · **Mehmet Emin Arslan[3]** · **Hakan Ozturk[2]** · **Aydin Demir[2]** · **Gokhan Dok[4]** · **Batuhan Aykanat[3]**

Muhammed Nadir Olabi
mnolabi@pm.me

Mehmet Emin Arslan
mehmeteminarslan@duzce.edu.tr

Hakan Ozturk
hakanozturk@sakarya.edu.tr

Aydin Demir
aydindemir@sakarya.edu.tr

Gokhan Dok
gokhandok@subu.edu.tr

Batuhan Aykanat
batuhanaykanat@duzce.edu.tr

1   Department of Civil Engineering, Institute of Natural Sciences, Sakarya University,
      54050 Sakarya, Turkey

2   Department of Civil Engineering, Faculty of Engineering, Sakarya University, 54050 Sakarya,
      Turkey

3   Department of Civil Engineering, Faculty of Engineering, Düzce University, 81620 Düzce, Turkey

4   Earthquake Studies Research and Application Center, Sakarya University of Applied Sciences,
      54050 Sakarya, Turkey